Over-Actuation Analysis and Fault-Tolerant Control of a Hybrid Unmanned Aerial Vehicle

Karl Frederik Prochazka, Tobias Ritz and Hugo Eduardo

Abstract Several reports like e.g. the *European Drones Outlook Study* predict that the number of unmanned aerial systems for commercial use will grow significantly within the next years. By further advancing in the direction of autonomous drone operation, it is most important to guarantee operational safety. Therefore, sophisticated methods of fault-tolerant control (FTC) have to be developed and tested. This paper presents a novel concept for determining the degree of a system's inherent over-actuation and how this information can be utilized for optimization-based control allocation in different modes of operation to achieve fault-tolerance. The paper describes the modeling and FTC of a dual system hybrid UAV, which is inherently over-acutated when in addition to the aerodynamic surfaces four lift rotors are used to control the aircraft during long range fixed-wing flight mode.

1 Introduction

In modern engineering applications many systems are inherently over-actuated, i.e. there are more control effectors than controlled variables available. This is especially true for aerospace systems, but also applies for example to robotic applications or the automotive sector as x-by-wire techniques are becoming more common. The resulting analytical actuator redundancy is often utilized for (in some prede-

Karl Frederik Prochazka
Institute of Flight Systems and Automatic Control, Otto-Berndt Strasse 2, 64287 Darmstadt, Germany e-mail: `prochazka@fsr.tu-darmstadt.de`

Tobias Ritz
Institute of Flight Systems and Automatic Control, Otto-Berndt Strasse 2, 64287 Darmstadt, Germany e-mail: `tobiasritz@t-online.de`

Hugo Eduardo
Institute of Flight Systems and Automatic Control, Otto-Berndt Strasse 2, 64287 Darmstadt, Germany e-mail: `eduardo@fsr.tu-darmstadt.de`

fined sense) optimized control distribution, which is widely used for fault-tolerant control to reallocate control signals among remaining healthy effectors in the face of actuator faults (see e.g. [14] [1] [9]). As the commercial drone market is expected to grow constantly within the near future [24] the research of sophisticated methods to achieve fault-tolerance and, at best, maintain nominal performance during the occurence of a fault is an important step to increase the overall operational safety for autonomous drone missions. Although there are different proposed ways for distribution and prioritizing amongst actuators in aircraft applications (e.g. minimal drag or radar signature [5] [8]) it would be interesting to generally determine the degree of over-actuation as a system property. This would yield more insight into how each individual control inputs contributes to the over-actuation and the information could thus be used for prioritizing of actuators and it could be considered during early development and system's design stages.

This paper presents a novel approach to analyze a system's degree of over-actuation from a system theory perspective regarding each individual system state and control input. The presented scheme can be seen as a variation of the classical controllability analysis explicitly regarding the concept of over-actuation for FTC purposes. The concept is applied to a dual system hybrid UAV which combines a multicopter's ability to take-off and land vertically with the energy efficient long-range flight capabilities of a conventional fixed-wing aircraft. To investigate the configuration's inherent over-acutation properties a UAV model has been developed which also considers the use of lift rotors during cruise flight. The concept of optimization-based control allocation has ben applied to that model enabling the control demands to be distributed among aerodynamic surfaces and lift rotors. Based on this progress a fault-tolerant control setup has been developed which achieves good tracking performance even in the face of severe faults in the aerodynamic control surfaces.

This paper is organized as follows. In Section 2 the proposed concept for over-actuation analysis is presented and the modeling procedure of the hybrid UAV on which the integrated FTC scheme has been simulated is described. Then the design of the FTC system, including the baseline feedback controller as well as the control allocation module, is presented. Section 3 describes the different experimental simulations and the results. Finally, Section 4 concludes the paper and gives an outlook on future research.

2 Materials and Methods

This sections begins by introducing the proposed method for determining a system's degree of over-actuation, which will later be applied to the hybrid UAV model. The modeling procedure of the UAV is presented in section 2.2. Section 2.3 describes the implemented fault-tolerant control approach to compensate for actuator faults.

2.1 Over-Actuation Analysis

In this section a novel concept to analyze a system's degree of over-actuation is presented, which utilizes classical controllability analysis techniques to explicitly take the concept of over-actuation for FTC purposes into account. A similar approach stemming from aircraft control was introduced in [7] and describes the so-called attainable moment space (AMS), which is used to determine the set of attainable moments or angular accelerations, respectively, for a given available actuator configuration. Although this method is also quite useful for FTC, it is primarily not thought of as an tool for over-actuation analysis. To introduce the proposed scheme first consider a linear system given in the state-space form

$$\dot{\mathbf{x}}(t) = \mathbf{A}\mathbf{x}(t) + \mathbf{B}\mathbf{u}(t) \tag{1}$$

$$\mathbf{y}(t) = \mathbf{C}\mathbf{x}(t) \tag{2}$$

with $\mathbf{x} \in \mathbb{R}^n$, $\mathbf{u} \in \mathbb{R}^m$ and $\mathbf{y} \in \mathbb{R}^p$. A system is then defined to be over-acutated if rank($\mathbf{B}$) is greater than the number of rows (n) of $\mathbf{B}$ [19]. However, for control purposes it is often of more importance to consider the controlled variables $\mathbf{y}$ and therefore a more specific definition of over-actuation will be used here (see e.g. [16]). Thus, a system is over-actuated (in the sense of anayltical redundancy) if it is functional controllable and has more inputs than outputs, that is

$$\text{rank}(\mathbf{S}_{OC}) = p \tag{3}$$

$$m > p \quad , \tag{4}$$

with the output controllability matrix

$$\mathbf{S}_{oc} = \begin{bmatrix} \mathbf{CB} \ \mathbf{CAB} \ \mathbf{CA}^2\mathbf{B} \ \dots \ \mathbf{CA}^{n-1}\mathbf{B} \end{bmatrix} \tag{5}$$

introduced by [23]. But, similar to the well known Kalman controllability criterion, this defintion gives only a binary result concerning a system's over-actuation and no further insight. The only other (to the author's knowledge) approach from [16] defines a system fullfilling $m > p$ and rank $\mathbf{B} > p$ to have $(m - p)$ degrees of actuator redundancy. The novel approach presented in this paper aims at assigning each individual controlled variable $\mathbf{y}$ a degree of over-actuation, as the over-actuation property does not necessarily hold true for every single output. For this purpose the positive semi-definite output controllability gramian

$$\mathbf{W_{oc}} = \mathbf{CW_cC^T} = \mathbf{C}\left(\int_0^\infty \mathbf{e}^{\mathbf{A}t}\mathbf{BB^T}\mathbf{e}^{\mathbf{A^T}t}\right)\mathbf{C^T} \tag{6}$$

is utilized. In adaption to the case of state controllability, described by $\mathbf{W_c}$, an output controllability ellipsoid in the state space can be defined from the matrix $\mathbf{W_{oc}}^{\frac{1}{2}}$ [6]. By performing a singular value decomposition of $\mathbf{W_{oc}}^{\frac{1}{2}}$

$$\mathbf{W_{oc}}^{\frac{1}{2}} = \mathbf{U\Sigma V^H} \tag{7}$$

with the matrix of left output singular vectors, $\mathbf{U} = [\mathbf{u_1}, \mathbf{u_2}, \ldots, \mathbf{u_p}]$, right input singular vectors, $\mathbf{V} = [\mathbf{v_1}, \mathbf{v_2}, \ldots, \mathbf{v_p}]$ and $\mathbf{\Sigma} = \mathrm{diag}(\sigma_1, \sigma_2, \ldots, \sigma_p)$ containing the singular values of $\mathbf{W_{oc}}^{\frac{1}{2}}$. Then the principal axes of the ellipsoid are given by $\mathbf{u_k}\sigma_\mathbf{k}$, describing the controllability of certain directions in the state space, that is, for a given $\|\mathbf{u}\| = 1$ the value $\sigma_\mathbf{k}$ describes how far we can go in the direction $\mathbf{u_k}$ [6]. To utilize this concept for over-actuation analysis first the nominal ellipsoid described by $\mathbf{\Sigma}_{nom}, \mathbf{U_{nom}}$ is calculated from (7). Then for each input $i \in 1, \ldots, m$ the corresponding reduced ellipsoid isdetermined by zeroing the column for actuator i from the input matrix

$$\mathbf{B_i} = [\mathbf{b_1}, \ldots, \mathbf{b_{i-1}}, \mathbf{0}, \mathbf{b_{i+1}}, \ldots, \mathbf{b_m}] \tag{8}$$

and scaling the reduced singular values obtained from

$$\mathbf{W_{oc,i}}^{\frac{1}{2}} = \left(\mathbf{C} \left(\int_0^\infty \mathbf{e^{At}B_iB_i^Te^{A^Tt}} \right) \mathbf{C^T} \right)^{\frac{1}{2}} = \mathbf{U_i\Sigma_iV_i^H} \tag{9}$$

with $\mathbf{\Sigma_i} = \mathrm{diag}(\sigma_{i,1}, \sigma_{i,2}, \ldots, \sigma_{i,p})$ to those of the nominal case. This leads to the following propositions:

Proposition 1 *A system is over-acutated regarding the output y_j with $j \in 1, \ldots, p$ if*

1. $\mathrm{rank}(\mathbf{S}_{OC}) = p$

2. $m > p$

3. for the corresponding singular values $\dfrac{\sigma_{i,j}}{\sigma_{j,nom}} > 0$ is true for all $i \in 1, \ldots, m$.

To determine how many actuators contribute to the over-actuation of an output y_j an individual *degree of over-actuation* for every y_j can be defined:

Proposition 2 *An over-actuated output y_j with $j \in 1, \ldots, p$ has a degree of over-actuation of τ_j, where τ_j is equal to the number of inputs $u_i, i \in 1, \ldots, m$ for which*

$$0 < \frac{\sigma_{i,j}}{\sigma_{j,nom}} < 1$$

applies.

Now also a statement regarding each individual actuator's contribution to the nominal control energy in every $\sigma_{j,nom}$-direction can be investigated by evaluating $\frac{\sigma_{i,j}}{\sigma_{j,nom}}$. Again in adaption to terms of *strong* and *weak* controllability from [6] an actuator's u_k contribution to the over-actuation of an output y_j can be termed stronger than that of another actuator u_l, if $\frac{\sigma_{k,j}}{\sigma_{j,nom}} \ll \frac{\sigma_{l,j}}{\sigma_{j,nom}}$ applies. Fig. 1 visualizes the concept of controllability ellipsoids for a three-dimensional case, i.e. $p = 3$.

To give an example the presented concept is applied to the ADMIRE (Aero-Data In Research Environment) aircraft benchmark model) [10]. The model has been widely used for FTC purposes due to it's large number of actuators (see e.g. [28][1]).
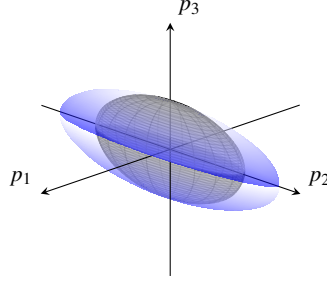
Fig. 1 Nominal (blue) and reduced (grey) controllability ellipsoids for an over-acutated system. The inner ellipsoid corresponds to the case where an actuator solely contributing to the over-actuation of output p_2 has been removed.

The seven control surfaces available for this example are: left and right canards (δ_{lc}, δ_{rc}) left and right outer elevons (δ_{loe}, δ_{roe}), left and right inner elevons (δ_{lie}, δ_{rie}) and rudder (δ_r). The model has been linearized for a straight level flight at the trim point $Ma = 0.22$, $h = 3000$ m with the given state vector $\mathbf{x}(t) = [V_{TAS} \; \alpha \; \beta \; p \; q \; r]^T \in \mathbb{R}^5$ containing the airspeed (V_{TAS}), angle of attack (α), angle of sideslip (β) and the angular velocities (p, q, r). The system outputs $\boldsymbol{\omega}(t) = [p \; q \; r]^T \in \mathbb{R}^3$. As the linearized model is open-loop unstable the corresponding eigenvalue of the system matrix has been shifted to the left half-plane in order to apply the presented concept. This is necessary, since by definition of $\mathbf{W_{oc}}$ in (6) it follows that the gramians only exist for stable systems, that is with the $\mathbf{A}$ matrix being Hurwitz.

For the example the inner and outer elevons and the canards are each ganged pairwise symetrically to generate pitch control, so that only the rudder produces control in yaw and roll direction (through roll-yaw coupling). Thus the effective vector of control inputs is reduced to $\mathbf{u}(t) = [\delta_c \; \delta_{ie} \; \delta_{oe} \; \delta_r]^T \in \mathbb{R}^4$. Figure 2 shows a bar diagram with the corresponding scaled singular values $\frac{\sigma_{i,j}}{\sigma_{j,nom}}$ for every output (p, q, r), so that the control energy contribution of each actuator is visualized. We can see that the largest singular value in the nominal case corresponds to the roll
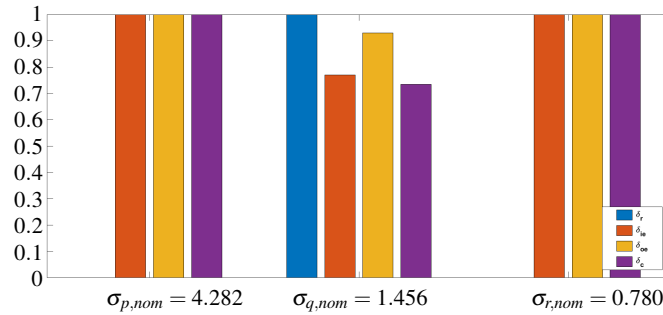
Fig. 2 Scaled singular values for the ADMIRE model with $p = 3$, $m = 4$ and all actuators ganged pairwise symmetrically.

axis, followed by pitch and yaw axis control. Although the system is over-actuated ($m = 4 > p$) all control inputs except the rudder only produce pitch control. Thus following the propositions from above the over-actuation of the system manifests only in the pitch rate q, which has a degree of over-acutation of $\tau_q = 3$. Regarding the indivual actuator's control energy contribution in q-direction it can also be seen that $\frac{\sigma_{\delta_c,q}}{\sigma_{q,nom}} < \frac{\sigma_{\delta_{ie},q}}{\sigma_{q,nom}} \ll \frac{\sigma_{\delta_{oe},q}}{\sigma_{q,nom}}$ which suggests that the outer elevons only have a minor influence on the overall pitch control.

2.2 Hybrid UAV modeling

The underlying configuration is a combination of a fixed-wing aircraft with the propulsion system of a multicopter. Such systems combine the ability to take-off and land vertically with the efficiency, the range and the velocity of a conventional fixed-wing aircraft. A major advantage of the discussed dual system compared to different available hybrid configurations (e.g. tilt-rotor or tilt-wing) is the combination of two independent propulsion systems. This avoids mechanical tilting mechanisms for the vertical take-off and landing capability, which result in non-input-affine system equations that are complicated to control during transition [15]. Another advantage lies in the fault-tolerant capabilities of such configurations due to the inherent over-actuation. This is given when in addition to the aerodynamic surfaces the lift rotors are utilized for motion control, which are generally disregarded during cruise flight. The novelty of this paper includes the analyzation of this system property and it's use for fault-tolerant control.

The state vector respresenting the UAV is

$$\mathbf{x}(t) = \begin{bmatrix} \mathbf{p} \ \boldsymbol{\Phi} \ \mathbf{v} \ \boldsymbol{\omega} \end{bmatrix}^{\mathrm{T}} \in \mathbb{R}^{12} \tag{10}$$

with the position $\mathbf{p} = \begin{bmatrix} x_n \ y_e \ z_d \end{bmatrix}^T$ given in the inertial system and the Euler angles $\Phi = \begin{bmatrix} \phi \ \theta \ \psi \end{bmatrix}^T$ with respect to the inertial system. The remaining states are the angular rates and translatory velocities $\omega = \begin{bmatrix} p \ q \ r \end{bmatrix}^T$ and $\mathbf{v} = \begin{bmatrix} u \ v \ w \end{bmatrix}^T$ of the UAV (see e.g. [25]). The system inputs are given as

$$\mathbf{u}(t) = \begin{bmatrix} \delta_e \ \delta_a \ \delta_r \ \delta_t \ \omega_1 \ \omega_2 \ \omega_3 \ \omega_4 \end{bmatrix}^{\mathrm{T}} \in \mathbb{R}^8 \tag{11}$$

with the aerodynamic control surfaces elevator (δ_e), ailerons (δ_a) and rudder (δ_r), the pusher rotor thrust (δ_t) and the four lift rotor's angular velocities (ω_1, ω_2, ω_3, ω_4). The mathematical model architecture developed in [22] is based on the equations presented in [2] and [25] with the final design of the hybrid UAV being a blend of two available configurations (*Texton Systems' Aerosonde HQ* and *Alti Transition*). Figure 3 shows the developed CAD model of the hybrid UAV airframe with the control inputs highlighted in blue. For the modeling procedure of the UAV a rigid-body
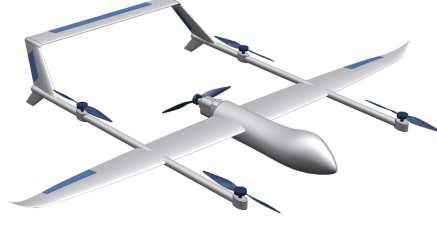
Fig. 3 CAD model of the dual system hybrid UAV airframe with the available control inputs marked in blue.

model is assumed with body movement being caused by forces and momentums resulting from aerodynamics, propulsion and gravity [22]. Further supposing the flat-earth assumption to be valid, the equations describing the motion of the dual system hybrid UAV in [22] are derived using the *Newton-Euler* formalism

$$
\begin{bmatrix} \mathbf{f} \\ \mathbf{m} \end{bmatrix} = \begin{bmatrix} m\mathbf{I}_{3\times3} & 0 \\ 0 & \mathbf{J} \end{bmatrix} \begin{bmatrix} \dot{\mathbf{v}} \\ \dot{\boldsymbol{\omega}} \end{bmatrix} + \begin{bmatrix} \boldsymbol{\omega} \times m\mathbf{v} \\ \boldsymbol{\omega} \times \mathbf{J}\boldsymbol{\omega} \end{bmatrix}
\tag{12}
$$

with $\mathbf{f}$ and $\mathbf{m}$ beeing the applied forces and moments [25]. The inertia tensor is represented by $\mathbf{J}$, $\boldsymbol{\omega}$ and $\mathbf{v}$ are the rotary and translatory velocities of the aircraft and m being the aircrafts mass. Applying (12) results in the following set (13) of nonlinear differential state equations.

$$
\begin{bmatrix} \dot{x}_n \\ \dot{y}_e \\ \dot{z}_d \end{bmatrix} = \begin{bmatrix} c_\theta c_\psi & s_\phi s_\theta c_\psi - c_\phi s_\psi & c_\phi s_\theta c_\psi + s_\phi s_\psi \\ c_\theta s_\psi & s_\phi s_\theta s_\psi + c_\phi c_\psi & c_\phi s_\theta s_\psi - s_\phi c_\psi \\ -s_\theta & s_\phi c_\theta & c_\phi c_\theta \end{bmatrix} \begin{bmatrix} u \\ v \\ w \end{bmatrix}
\tag{13a}
$$

$$
\begin{bmatrix} \dot{\phi} \\ \dot{\theta} \\ \dot{\psi} \end{bmatrix} = \begin{bmatrix} 1 & \sin\phi \tan\theta & \cos\phi \tan\theta \\ 0 & \cos\phi & -\sin\phi \\ 0 & \dfrac{\sin\phi}{\cos\theta} & \dfrac{\cos\phi}{\cos\theta} \end{bmatrix} \begin{bmatrix} p \\ q \\ r \end{bmatrix}
\tag{13b}
$$

$$
\begin{bmatrix} \dot{u} \\ \dot{v} \\ \dot{w} \end{bmatrix} = \begin{bmatrix} rv - qw \\ pw - ru \\ qu - pv \end{bmatrix} + \frac{1}{m} \begin{bmatrix} f_x \\ f_y \\ f_z \end{bmatrix}
\tag{13c}
$$

$$
\begin{bmatrix} \dot{p} \\ \dot{q} \\ \dot{r} \end{bmatrix} = \begin{bmatrix} \frac{J_{xz}(J_x - J_y + J_z)}{\Gamma} pq - \frac{J_z(J_z - J_y) + J_{xz}^2}{\Gamma} qr + \frac{J_z}{\Gamma} l + \frac{J_{xz}}{\Gamma} n \\ \frac{J_z - J_x}{J_y} rp - \frac{J_{xz}}{J_y} \left(p^2 - r^2 \right) + \frac{m}{J_y} \\ \frac{J_x(J_x - J_y) + J_{xz}^2}{\Gamma} pq - \frac{J_{xz}(J_x - J_y + J_z)}{\Gamma} qr + \frac{J_{xz}}{\Gamma} l + \frac{J_x}{\Gamma} n \end{bmatrix}
\tag{13d}
$$

The applied forces are

$$
\mathbf{f} = \begin{bmatrix} f_x \\ f_y \\ f_z \end{bmatrix} = \mathbf{f}_g + \mathbf{f}_{p,lift} + \mathbf{f}_{p,pusher} + \mathbf{f}_a
\tag{14}
$$

Table 1 Mass and geometric properties measured from the developed CAD model.

Parameter	Description	Value	Unit
m	mass	15.5	kg
J_x	moment of inertia about body x-axis	1.545	kgm^2
J_y	moment of inertia about body y-axis	1.856	kgm^2
J_z	moment of inertia about body z-axis	3.161	kgm^2
J_{xz}	xz product of inertia	0.1204	kgm^2
S	wing area	0.55	m^2
b	wing span	2.89	m
$\bar{c}$	mean aerodynamic chord length	0.189	m
d_x	rotor distance in body x-direction from CG[1]	0.6	m
d_y	rotor distance in body y-direction from CG[1]	0.6	m

[1] Center of gravity

taking into account the gravitational force as well as the propulsion forces of the lift and pusher motors. The applied moments are

$$\mathbf{m} = \begin{bmatrix} l \\ m \\ n \end{bmatrix} = \mathbf{m}_a + \mathbf{m}_{p,lift} \tag{15}$$

taking into account aerodynamic effects and the moments generated by the lift rotors. The geometric and mass properties of the UAV calculated from the CAD model shown in fig. 3 are given in table 1. Usually after the transition from hover to cruise flight is finished for such dual system UAVs the lift rotors are fixed in a minimal-drag position and only used again for the next transition phase from cruise flight back to quadcopter hover mode [11]. Therefore, no available models are known to determine the lift rotors effectiveness when they are turned on during cruise flight. To investigate the complex aerodynamic effects taking place during hover and transition mode a modified instationary vortex-lattice method has been developed in [12].

For the purpose to capture the control effectiveness of the lift rotors and the induced aerodynamic coupling effects during cruise flight for this paper *computational fluid dynamics* (CFD) simulations have been performed in *Ansys Fluent 19.0*. Figure 4 shows the velocity flow field for a free-stream velocity of $V_{TAS} = 30\,\mathrm{m\,s^{-1}}$ and a lift rotor angular velocity of $\omega = 6000\,\mathrm{rpm}$ for a half-segment CAD model of the UAV with reduced complexity. The plots suggest that the incident flow of the lift rotors differs and that they will have an effect on the overall aerodynamic behaviour of the UAV. Due to the large number of required simulations and long computation times when using the lift rotors in CFD, first only the longitudinal motion of the UAV has been modeled. The applied aerodynamic drag and lift forces (f_D, f_L) and the pitch moment (m) are

$$f_D = \bar{q}SC_D \quad , \quad f_L = \bar{q}SC_L \quad , \quad m = \bar{q}S\bar{c}C_M \tag{16}$$
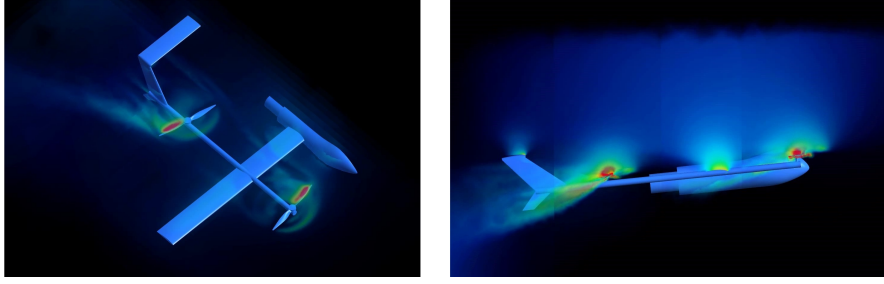
Fig. 4 CFD simulation of the hybrid UAV for $V_{TAS} = 30\,\mathrm{m\,s}^{-1}$ and $\omega = 6000\,\mathrm{rpm}$. Red areas indicate the maximum velocity of $V_{TAS,\mathrm{max}} \approx 50\,\mathrm{m\,s}^{-1}$ on the lift rotors.

with the dynamic pressure $\bar{q} = \frac{1}{2}\rho V_{TAS}^2$ and the air density ρ. With the angle of attack (α) and the angle of sideslip (β) the total force and moment coefficients for the longitudinal motion are assumed to be:

$$
\begin{aligned}
C_D =& C_{D_0} + C_{D_{\alpha,1}} \cdot \alpha + C_{D_{\alpha,2}} \cdot \alpha^2 + C_{D_{\omega,front,1}} \cdot (\omega_1 + \omega_2) + \\
& + C_{D_{\omega,front,2}} \cdot (\omega_1^2 + \omega_2^2) + C_{D_{\omega,back,1}} \cdot (\omega_3 + \omega_4) + C_{D_{\omega,back,2}} \cdot (\omega_3^2 + \omega_4^2)
\end{aligned}
\tag{17}
$$

$$
\begin{aligned}
C_L =& C_{L_0} + C_{L_\alpha} \cdot \alpha + C_{L_{\delta_e}} \cdot \delta_e + C_{L_{\omega,front,1}} \cdot (\omega_1 + \omega_2) + \\
& + C_{L_{\omega,front,2}} \cdot (\omega_1^2 + \omega_2^2) + C_{L_{\omega,back,1}} \cdot (\omega_3 + \omega_4) + C_{L_{\omega,back,2}} \cdot (\omega_3^2 + \omega_4^2)
\end{aligned}
\tag{18}
$$

$$
\begin{aligned}
C_M =& C_{M_0} + C_{M_\alpha} \cdot \alpha + C_{M_q} \cdot q^* + C_{M_{\delta_e}} \cdot \delta_e + C_{M_{\omega,front,1}} \cdot (\omega_1 + \omega_2) + \\
& + C_{LM_{\omega,front,2}} \cdot (\omega_1^2 + \omega_2^2) + C_{M_{\omega,back,1}} \cdot (\omega_3 + \omega_4) + C_{M_{\omega,back,2}} \cdot (\omega_3^2 + \omega_4^2)
\end{aligned}
\tag{19}
$$

with $q^* = \frac{\bar{q}\bar{c}}{2V_{TAS}}$. The dimensionless aerodynamic stability and control derivatives from (17) - (19) have been found by performing regression analysis of the acquired force and moment data from CFD analysis and are given in the appendix. Notice that the derivatives for the front (ω_1, ω_2) and back (ω_3, ω_4) lift rotors are the same, since for longitudinal motion they are controlled pairwise identically. The pitch damping coefficient C_{M_q} has been taken from a similar configuration in [2] as it cannot be directly determined from the static moments calculated in the CFD simulations. However, according to [25] it can be approximated by using the UAV's tail lift coefficient, which is scheduled for the next modeling process.

2.3 Control Law Design

If a system is over-actuated (see section 2.1) the resulting redundancy can be utilized to increase the overall safety of a system and maintain, at best, nominal performance
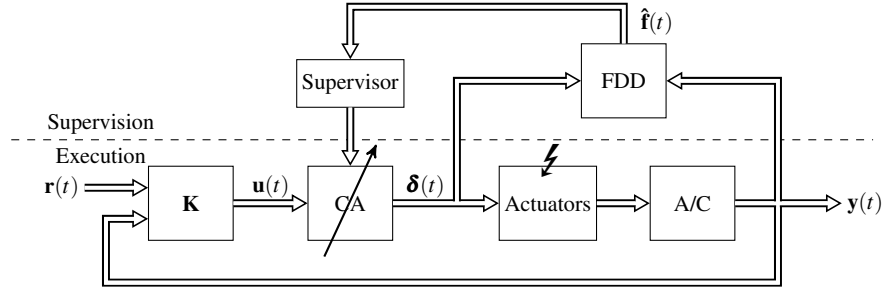
Fig. 5 General structure of an AFTC System with actuator faults and Control Allocator (CA).

of the fault-free case even in the presence of system faults or failures. Therefore, Fault Tolerant Control (FTC) systems have to be implemented. These can generally be divided into two groups, namely active (AFTC) and passive (PFTC) systems [3]. For PFTC systems a fixed controller structure is used and presumed faults as well as system uncertainties are considered in a robust design approach. On the contrary, an AFTC system poses a more flexible structure as it reacts to the occurence of previously unknown system faults in real-time and changes the underlying controller structure. This enables the system not only to be stabilized but also to consider the actual fault status to achieve (in some pre-defined sense) optimal performance. However, this typically requires at least two additional elements: a fault detection and diagnosis (FDD) mechanism and a supervisor module, which reconfigurates the controller based on the fault information from the FDD. For more information on PFTC and AFTC see for example [3][27].

In this paper, to control the hybrid UAV described in section 2.2, an AFTC scheme has been used, consisting of a *Control Allocator* (CA) and a *Dynamic Inversion* (DI) based control law. A CA module is traditionally used in over-actuated aircraft systems to distribute the control inputs, or virtual controls $u(t)$, over the redundant true control surfaces $\delta(t)$ (see e.g. [4][7]). This has the advantage that in the case of an actuator fault the CA distribution law is reconfigured while the baseline controller (K) remains unaltered. In fig. 5 the general structure of the implemented AFTC system is shown. The focus of this paper lies in the novel approach to apply FTC to a hybrid UAV by utilizing the quad rotors in cruise flight for achieving over-actuation in the rotary degrees of freedom. Therefore the fault signal from the FDD is assumed to be ideal and available to the CA module as soon as the fault occurs. This is a typical approach for evaluating FTC concepts [28][26]. Nevertheless this approach is a simplification of the reality, because robustness of an FDD e.g. against model uncertainties is a serious issue which has to be examined in future works.

Control Allocator Design

Consider a linear system given in the state-space form of (1), (2) with a slightly different notation:

$$\dot{\boldsymbol{x}}(t) = \boldsymbol{A}\boldsymbol{x}(t) + \boldsymbol{B}\boldsymbol{\delta}(t) \tag{20}$$

$$\boldsymbol{y}(t) = \boldsymbol{C}\boldsymbol{x}(t) \tag{21}$$

with the state vector $\boldsymbol{x} \in \mathbb{R}^n$, $\boldsymbol{\delta} \in \mathbb{R}^m$ being the true (physical) control inputs and $\boldsymbol{y} \in \mathbb{R}^p$ the outputs. If the system (20), (21) is over-actuated according to (3) - (4), that is $p < m$, first a baseline controller $\mathbf{K}$ can be designed with the control signals, or virtual controls, $\boldsymbol{u} \in \mathbb{R}^k$ and $k < m$ (where here $k = p$ is assumed), disregarding the number of true control inputs $\boldsymbol{\delta}(t)$. A Control Allocator (CA) module then distributes the virtual controls over the true controls of the system, so that with the given output control effectiveness matrix $\boldsymbol{CB} \in \mathbb{R}^{p \times m}$ the control allocation problem can be formulated as the search for $\boldsymbol{\delta}(t)$, such that

$$\boldsymbol{CB}\boldsymbol{\delta}(t) = \boldsymbol{u}(t)$$
$$\text{s.t.} \quad \boldsymbol{\delta}_{min} \leq \boldsymbol{\delta} \leq \boldsymbol{\delta}_{max} \quad . \tag{22}$$

While there are different approaches for solving this control allocation problem [17] the methods of optimization based control allocation implemented for this paper are of special interest. They allow (similar to LQR regulators) performance weighting of certain actuators while minimizing a given p-norm cost function J [13]. For the formulation of J different constraints like actuator deflection or rate limits can also be included in the optimization process. This CA method can then be used to re-allocate the virtual controls after an actuator fault has been detected to achieve fault-tolerance, while the underlying controller $\mathbf{K}$ does not need to be reconfigured. The optimization-based approach offers the advantage that the redundant control signals can also be distributed in a fault-free case in order to fulfill secondary objectives like e.g. minimizing the actuator's control deflection [19]. When the 2-norm is used for J, the optimization-based CA problem can be converted into a quadratic program (QP) for which a global solution can be found [20]. The problem can then be stated in a sequential form where in a first step the following cost function is minimized:

$$\min \quad J = \|\mathbf{W}_u(\mathbf{CB}\boldsymbol{\delta}_u(t) - \boldsymbol{u}(t))\|_2$$
$$\text{s.t.} \quad \boldsymbol{\delta}_{min} \leq \boldsymbol{\delta} \leq \boldsymbol{\delta}_{max} \tag{23}$$

where $\boldsymbol{\delta}_u(t)$ is a feasible solution minimizing the difference $\mathbf{CB}\boldsymbol{\delta}(t) - \boldsymbol{u}(t)$ if the desired virtual control input $\boldsymbol{u}(t)$ is attainable. The weighting matrix $\mathbf{W}_u$ is included for prioritization among the individual virtual controls. If the commanded virtual control $\boldsymbol{u}(t)$ proves to be attainable with the available actuators, secondary optimization objectives can be introduced by solving a second optimization problem

$$\min \quad J = \|\mathbf{W}_\delta(\boldsymbol{\delta}(t) - \boldsymbol{\delta}_p(t))\|_2$$
$$\text{s.t.} \quad \mathbf{CB}\boldsymbol{\delta}(t) = \mathbf{u}(t)$$
$$\boldsymbol{\delta}_{min} \leq \boldsymbol{\delta} \leq \boldsymbol{\delta}_{max} \tag{24}$$

where the difference between the solution $\boldsymbol{\delta}(t)$ and a preferred true control vector $\boldsymbol{\delta}_p(t)$ is minimized. $\boldsymbol{\delta}_p(t)$ is in general required to be defined in each iteration

but assumed to be constant ($\boldsymbol{\delta}_p(t) = \mathbf{0}$) for all the simulations performed in this work. The weighting matrix $\mathbf{W}_\delta$ in (24) also allows for the prioritization of certain actuators. Several numerical algorithms for the implementation of CA posed as a constrained QP problem have already been evaluated and compared in the past [20]. In this work the active-set algorithm has been used for the implementation of optimal CA module since it is computationally efficient for systems with a medium number of true controls ($m \approx 10$) and has good convergence properties [14].

Dynamic Inversion Control

As a baseline feedback controller the *Nonlinear Dynamic Inversion* (NDI) technique has been employed, which is based on the feedback linearization approach [25]. The NDI method is very popular in aircraft systems since it is suitable for a wide range of operating conditions by taking into account strong nonlinearities of the aircraft [8][25]. Furthermore the technique can be employed for a wide variety of system types and is naturally well suited for the design in combination with a control allocation module. It is also possible to assign specific closed-loop dynamics in order to achieve desired system responses, which satisfy typical flying qualities specifications [18]. For a plant given in the nonlinear state-variable form

$$\dot{\mathbf{x}}(t) = \mathbf{f}(\mathbf{x}(t)) + \mathbf{g}(\mathbf{x}(t))\mathbf{u}(t) \tag{25}$$
$$\mathbf{y}(t) = \mathbf{h}(\mathbf{x}(t)) \tag{26}$$

and with reference inputs $\mathbf{r}(t) \in \mathbb{R}^p$ the overall NDI controller, when combined with a control allocator, is thus given by

$$\boldsymbol{u}(t) = \dot{\boldsymbol{r}}_{ref}(t) + \mathbf{v}(t) - \mathbf{F}(\mathbf{x}(t)) \quad . \tag{27}$$

Here $\mathbf{F}(\mathbf{x}(t))$ is a full state variable feedback used for linearization. For perfect inversion this makes the plant from $\mathbf{v}(t)$ to $\mathbf{y}(t)$ be a simple linear system with p integrators in parallel [25]. If the plant is given in linear form (20), (21) for $\mathbf{F}(\mathbf{x}(t)) = \mathbf{CA} \in \mathbb{R}^{p \times n}$ applies, so that the control input becomes

$$\boldsymbol{u}(t) = \dot{\boldsymbol{r}}_{ref}(t) + \mathbf{v}(t) - \mathbf{CAx}(t) \quad . \tag{28}$$
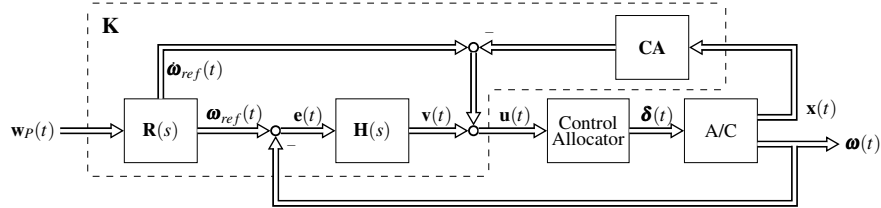
Fig. 6 NDI control structure with Control Allocator (CA) module for a linearized model.

The control allocation module then distributes the virtual control input $\boldsymbol{u}(t) \in \mathbb{R}^p$ from (28) over the true controls $\boldsymbol{\delta}(t) \in \mathbb{R}^m$, in this case the aircraft's actuators and quad rotors, using an optimization technique as described in the previous section.

Fig. 6 shows the overall control structure used in this work. For such a setup the controlled variables consist of the angular velocities $\boldsymbol{\omega} = [p\ q\ r]^{\mathrm{T}} \in \mathbb{R}^3$ and through the use of appropriate reference models $\mathbf{R}(s) = \mathrm{diag}(R_p(s), R_q(s), R_r(s)) \in \mathbb{C}^{3\times3}$ desired aircraft dynamics $\boldsymbol{\omega}_{ref} \in \mathbb{R}^3$ are generated from pilot input commands $\mathbf{w}_P \in \mathbb{R}^3$. The reference models are designed in order to satisfy standard forms for the aircraft modes (see e.g. [18]). Additionally the feedforward input $\dot{\boldsymbol{\omega}}_{ref} \in \mathbb{R}^3$ improves tracking behaviour of the closed-loop system. The control structure further consists of the inner control loop **CA** and the outer control loop including the stabilizing compensator $\mathbf{H}(s) = \mathrm{diag}(H_p(s), H_q(s), H_r(s)) \in \mathbb{C}^{3\times3}$, which has been implemented as a typical PI controller to reject disturbances and inaccuracies in the modelled aircraft dynamics.

3 Simulation and Results

For the following investigations the hybrid UAV model described in 2.2 has been trimmed and linearized for a horizontal flight at $h = 50\,\mathrm{m}$ and $V_{TAS} = 30\,\mathrm{m\,s^{-1}}$ with the longitudinal motion state vector

$$\mathbf{x_L}(t) = \begin{bmatrix} u\ w\ q\ \theta \end{bmatrix}^{\mathrm{T}} \in \mathbb{R}^4 \tag{29}$$

containing the longitudinal and vertical velocities (u, w) in the aircraft body coordinates, the pitch rate (q) and the Euler pitch angle (θ). The control inputs are given as

$$\mathbf{u_L}(t) = \begin{bmatrix} \delta_e\ \delta_t\ \delta_{\omega,\mathrm{front}}\ \delta_{\omega,\mathrm{back}} \end{bmatrix}^{\mathrm{T}} \in \mathbb{R}^4 \tag{30}$$

with the elevator (δ_e), pusher thrust (δ_t) , the front lift rotors $(\delta_{\omega,\mathrm{front}} = \omega_1 + \omega_2)$ and the back lift rotors $(\delta_{\omega,\mathrm{back}} = \omega_3 + \omega_4)$. This notation for the lift rotors has been chosen since for pure longitudinal motion the front and lift rotors are controlled pairwise identically and the corresponding control derivatives have the same value. With the pitch rate (q) as output variable the resulting state space model is

$$\mathbf{A_L} = \begin{bmatrix} -0.326 & 0.485 & -1.646 & -9.792 \\ -0.528 & -2.291 & 29.955 & -0.538 \\ 0.022 & -0.391 & -0.352 & 0 \\ 0 & 0 & 1 & 0 \end{bmatrix} \tag{31a}$$

$$\mathbf{B_L} = \begin{bmatrix} -0.385 & 45.355 & -2.06 & -1.49 \\ 6.998 & 0 & -7.48 & -12.15 \\ -15.439 & 0 & 48.8 & -44.2 \\ 0 & 0 & 0 & 0 \end{bmatrix} \tag{31b}$$

$$\mathbf{C_L} = \begin{bmatrix} 0\ 0\ 1\ 0 \end{bmatrix} \tag{31c}$$

The remainder of this section is divided into two parts: First the concept presented in section 2.1 is applied to the longitudinal UAV model (31) to determine the degree of over-acutation for the rotatory degree of freedom in pitch direction and the lift rotor's contribution. In the second part closed-loop simulations are presented where the ability of the optimization-based CA method integrated in the FTC setup from section 2.3 to utilize different inputs for pitch control is shown. Afterwards the fault-tolerance capabilities of the hybrid UAV in combination with optimal CA is demonstrated and the closed-loop performance of the fault-tolerant control scheme investigated.

3.1 Over-Actuation analysis of the hybrid UAV

For the over-actuation analysis according to 2.1 the scaled singular values for the state space model 31 are determined. Because $y(t) = q(t)$ and $m = 4$ with rank$(\mathbf{B_L}) = 3$, rank$(\mathbf{S_{OC}}) = p = 1$ the system is clearly over-actuated (see (3)-(4)). Figure 7 shows the scaled singular values $\frac{\sigma_{i,q}}{\sigma_{q,nom}}$ for the pitch degree of freedom. As expected the pusher thrust (δ_t) has no contribution to pitch control ($\frac{\sigma_{\delta_t,q}}{\sigma_{q,nom}} = 1$), because the pusher motor is assumed to be aligned with the body x-axis and thus produces no torque around the pitch axis. It can furhter be seen that the pitch rate q has a degree of over-actuation of $\tau_q = 3$, because all the remaining control inputs (δ_e, $\delta_{\omega,\text{front}}$, $\delta_{\omega,\text{back}}$) contribute to it's total control energy. Regarding their individual control energy distribution $\frac{\sigma_{\delta_{\omega,\text{front}},q}}{\sigma_{q,nom}} < \frac{\sigma_{\delta_{\omega,\text{back}},q}}{\sigma_{q,nom}} < \frac{\sigma_{\delta_e,q}}{\sigma_{q,nom}}$ suggests that the lift rotors have an even stronger influence on pitch control than the elevator. The fact that the scaled singular values for the front and back lift rotors differ from each other is in accordance with the CFD simulation results and resulting entries in the corresponding columns of $\mathbf{B_L}$. It is assumed that this results from non-neglectable aerodynamic cross-coupling effects between the lift rotors and the wing influencing the effective incident flow of the rotor plains.
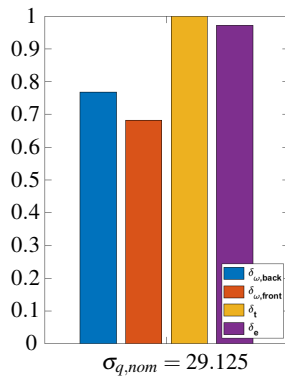

Fig. 7 Scaled singular values for the longitudinal hybrid UAV model with $p = 1$ and $m = 4$.

3.2 Closed-Loop Simulations

In the next simulations the closed-loop performance of the FTC setup described in 2.3 combined with an optimization-based control allocator (CA) is presented. Because only longitudinal control is assumed, the pitch rate (q) has been chosen as the controlled variable. The UAV model has been expanded to also contain actuator dynamics, represented by first oder lag transfer functions with a static gain of $K = 1$ and a time constant of $T = 0.05\,$s, and saturation elements taking into the account the limits for the elevator's deflection angle and the lift rotor's angular velocities. The corresponding minimum and maximum values are given by ($\delta_{e,\mathrm{min}} = -30\,$deg, $\delta_{e,\mathrm{max}} = 30\,$deg) and ($\omega_{\mathrm{min}} = 0\,$rpm, $\omega_{\mathrm{max}} = 10000\,$rpm). The reference model and resulting PI feedback controller for the pitch axis are based on [18] and given by

$$R_q(s) = \frac{4}{s^2 + 3.4s + 4} \quad , \quad H_q(s) = \frac{3.4s + 4}{s} \quad . \tag{32}$$

To make the simulation results comparable for every scenario the same reference signals have been commanded. Therefore, the UAV is excited in the pitch axis by a pilot step command of $40\,$deg$/$s ($t = 1 - 3.5$s) and $-40\,$deg$/$s ($t = 3.5 - 6$s). The simulations have been performend in *MATLAB/Simulink* with a fixed simulation step size of $\Delta t = 0.01\,$s using the *ode4* (Runge-Kutta) solver.

Control Allocator Simulation

In this scenario the capability of the implemented CA method to consider secondary objectives for the prioritization among different actuators is presented. Here no acutator faults are assumed. As there is only one virtual control for the pitch axis ($\mathbf{u} \in \mathbb{R}^1$) no weight amongst $\mathbf{u}$ is necessary, that is $\mathbf{W}_u = 1$. In order to make the CA module only utilize the elevator or lift rotors, the respective weighting matrices $\mathbf{W}_\delta$ from (24) have been selected as follows:

$$\mathbf{W}_{\delta,\delta_{\mathbf{e}}} = \begin{bmatrix} 1 & 0 & 1000 & 1000 \end{bmatrix} \quad , \quad \mathbf{W}_{\delta,\omega} = \begin{bmatrix} 1000 & 0 & 1 & 1 \end{bmatrix} \quad . \tag{33}$$

Figure 8 shows the commanded step input and reference signal generated by $R_q(s)$ and compares them to the controlled variables from the two scenarios with different CA weights. The plot further shows the resulting control inputs. It can be observed that the CA algorithm distributes the control signals according to the selected weights by either using the elevator (without lift rotors) or the front and back lift rotors (without elevator) to generate the required pitch signal. Secondly, It can be noticed that the front and back rotors require different angular velocities to follow a reference pitch rate with the same absolut value around the positive and negative pitch axis, respectively. For both scenarios good reference tracking is achieved.
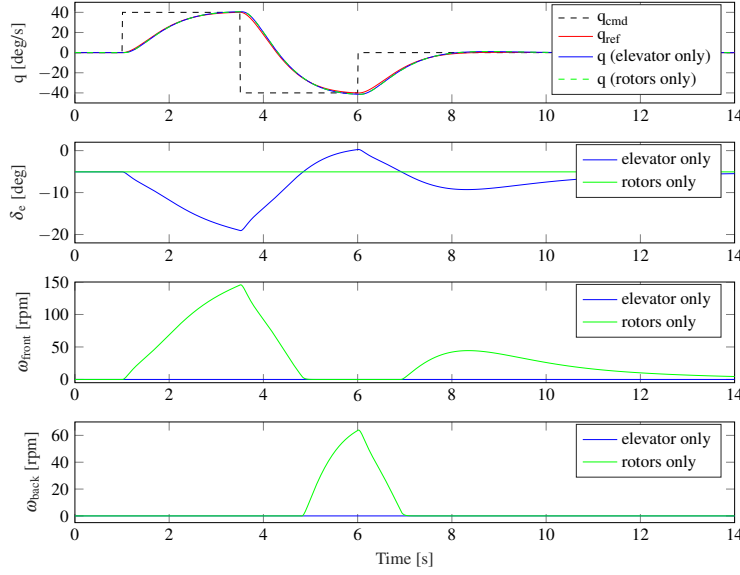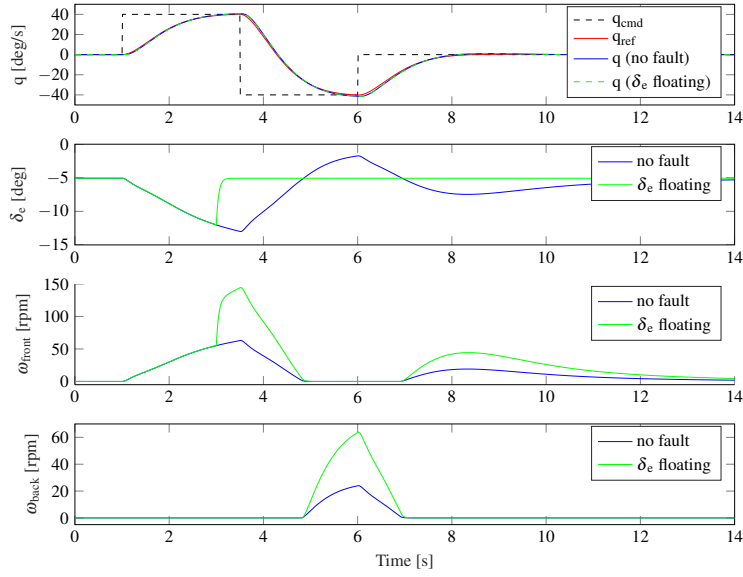
Fig. 8 Reference signals, controlled variable (q) and control signals (δ_e, $\delta_{\omega,\text{front}}$, $\delta_{\omega,\text{back}}$) produced by different CA weights.

Fault-Tolerant Control Simulation

Here the fault-tolerance performance of the FTC setup with optimal CA is presented. For the following the simulations the weighting matrix $\mathbf{W}_\delta = \begin{bmatrix} 1 & 0 & 5 & 5 \end{bmatrix}$ has been selected to utilize both elevators and lift rotors for pitch control. Figure 9 shows the simulation results for the fault-free case and a scenario where a floating fault (total loss of effectiveness) of the elevator occurs at $t = 3\,\text{s}$. Based on the available fault information the CA module reallocates the control inputs amongst the lift rotors leading to an increased control demand for $\delta_{\omega,\text{front}}$ and $\delta_{\omega,\text{back}}$. Despite the total failure of δ_e the reference signal can be tracked without any sign of performance loss visible. In the next scenario a jamming fault of δ_e has been simulated $t = 1.8\,\text{s}$ with the elevator being stuck at $\delta_{e,\text{fault}} = -8\,\text{deg}$. In figure 10 it can be seen the lift rotors are able to compensate for the elevator fault and the reference signal is tracked quite accurately. It can further be noticed that due to the constant (unwanted) pitch up torque from the elevator the back lift rotors have to generate more thrust than in the previous fault scenario and deliver a constant input of $\delta_{\omega,\text{back}} \approx 30\,\text{rpm}$ to compensate the elevator torque in steady-state flight. In table 2 the RMS and maximum absolute value of the control error for the different scenarios (prioritization of δ_e and δ_ω respectively, weights on both δ_e and δ_ω, floating and jamming fault for δ_e) are given. It can be seen that the error for the FTC setup with actuator failures does not significantly exceed the fault-free scenarios. This shows the effectiveness of the implemented FTC with optimal control allocation and (assuming ideal FDD) the good performance of the lift rotors when being utilized for fault-tolerant control.

Fig. 9 Reference signals, controlled variable (q) and control signals (δ_e, $\delta_{\omega,\text{front}}$, $\delta_{\omega,\text{back}}$) for fault-free case and floating fault in δ_e.
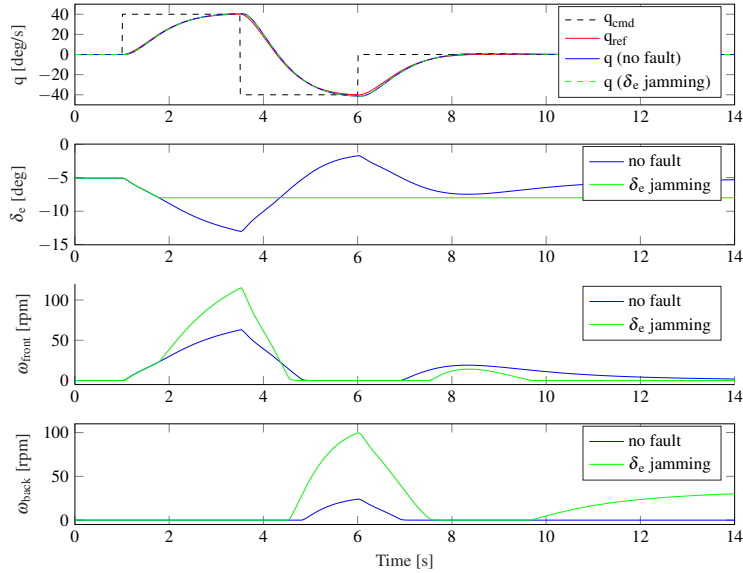
Fig. 10 Reference signals, controlled variable (q) and control signals (δ_e, $\delta_{\omega,\text{front}}$, $\delta_{\omega,\text{back}}$) for fault-free case and jamming fault of δ_e.

Table 2 RMS and maximum absolute value of the control error for different scenarios.

Scenario	δ_e only	δ_ω only	δ_e and δ_ω	δ_e and δ_ω (floating)	δ_e and δ_ω (jamming)
e_{RMS}	0.8021	0.8387	0.8174	0.823	0.8413
$e_{\max}$	2.451	2.504	2.474	2.454	2.495

4 Conclusions and Future Work

In this paper, a new approach to determine a system's degree of over-actuation has been proposed, which represents a variation of the classical controllability analysis explicitly regarding the concept of over-actuation for FTC purposes. The presented analysis method has been applied to a dual system hybrid UAV model. A further novelty presented in this work is the utilization of the UAV's inherent over-actuation by using it's four lift rotors, which are typically only employed for hover and transition mode, for pitch control during cruise flight. First promising simulation results with a linearized model have been presented, in which a control allocation module was able to distribute the virtual control effort among the aerodynamic surfaces and lift rotors so that good reference tracking has been achieved even in the face of severe actuator failures. The presented approach can potentially increase the overall operational safety of hybrid UAVs while performing missions during long range fixed-wing flights. Future work will include the conduction of further CFD simulations to also model the lateral-directional behaviour of the UAV as well as adding a module for fault detection and diagnosis (FDD) to the FTC scheme, which has already been presented in ([21]. Because FDD methods are very sensitive to uncertainties, e.g. coming from inevitable discrepancies between CFD data and true aerodynamic properties, their robustness properties have to be examined thoroughly. As the proposed FTC concept focuses on LTI models a generalised LPV model based extension seems useful. Furthermore, it is planned to perform hardware-in-the-loop (HiL) simulations to verify the real-time capabilities of the implemented FTC structure.

Appendix

Table 3 Aerodynamic derivatives for the longitudinal motion derived from CFD simulations.

Derivate	Value	Derivative	Value
C_{D_0}	0.038	$C_{L_{\omega,front,2}}$	$6.8000e-09$
$C_{D_{\alpha,1}}$	0.000318	$C_{L_{\omega,back,1}}$	$6.1907e-05$
$C_{D_{\alpha,2}}$	0.001195	$C_{L_{\omega,back,2}}$	$9.1403e-09$
$C_{D_{\omega,front,1}}$	$1.2696e-05$	C_{M_0}	0.3706
$C_{D_{\omega,front,2}}$	$1.1e-11$	C_{M_α}	-0.1112
$C_{D_{\omega,back,1}}$	$1.1081e-05$	C_{M_q}	-3.6 (taken from [4])
$C_{D_{\omega,back,2}}$	$6.4967e-10$	$C_{M_{\delta_e}}$	-0.0892
C_{L_0}	0.3131	$C_{M_{\omega,front,1}}$	$1.5791e-04$
C_{L_α}	0.0960	$C_{M_{\omega,front,2}}$	$5.7193e-08$
$C_{L_{\delta_e}}$	0.0105	$C_{M_{\omega,back,1}}$	$-1.4313e-04$
$C_{L_{\omega,front,1}}$	$3.7790e-05$	$C_{M_{\omega,back,2}}$	$-5.8937e-08$

References

[1] C. Alwi, H.and Edwards and C. Pin Tan. *Fault Detection and Fault-Tolerant Control Using Sliding Modes*. SpringerLink Bücher. Springer-Verlag London Limited, London, 2011.

[2] R. Beard and T. McLain. *Small Unmanned Aircraft: Theory and Practice*. Princeton University Press, Princeton, 2012.

[3] M. Blanke, M. Kinnaert, and J. Lunze. *Diagnosis and fault-tolerant control*. Third edition edition, 2016.

[4] J. Buffington. Modular control law design for the innovative control effectors (ice) tailless fighter aircraft configuration 101-3.

[5] J. Buffington, P. Chandler, and M. Pachter. On-line system identification for aircraft with distributed control effectors. *International Journal of Robust and Nonlinear Control 9*, pages 1033–1049, 1999.

[6] G. Dullerud and F. Paganini. *A Course in Robust Control Theory: A Convex Approach*, volume 36 of *Texts in Applied Mathematics*. Springer NY, 2010.

[7] W. Durham. Constrained control allocation. *Journal of Guidance, Control, and Dynamics*, 16(4):717–725, 1993.

[8] W. Durham, K. Bordignon, and R. Beck. *Aircraft Control Allocation*. John Wiley & Sons, Ltd, Chichester, UK, 2016.

[9] C. Edwards and C. Alwi, H.and Tan. Sliding mode methods for fault detection and fault tolerant control with application to aerospace systems. *International Journal of Applied Mathematics and Computer Science*, 22(1):499, 2012.

[10] L. Forssell and U. Nilsson. Admire the aero-data model in a research environment version 4.0, model description. 2005.

[11] Airbus Group. Quadcruiser - an innovative hybrid aircraft concept. Brochure, 2015.

[12] M. Haimerl, F. Binz, S. Engels, and D. Morrmann. Entwicklung einer modifizierten, instationären wirbelgittermethode für eine senkrechtstartfähige flugzeugkonfiguration. 2017.

[13] O. Harkegard. Efficient active set algorithms for solving constrained least squares problems in aircraft control allocation. In *Proceedings of the 41st IEEE Conference on Decision and Control*, pages 1295–1300, Piscataway, NJ, 2002. IEEE.

[14] O. Härkegård. *Backstepping and control allocation with applications to flight control*. PhD thesis, Linköping University, 2003.

[15] P. Hartmann, C. Meyer, and D. Moormann. Unified velocity control and flight state transition of unmanned tilt-wing aircraft. *Journal of Guidance, Control, and Dynamics*, 40(6):1348–1359, 2017.

[16] Q. Jiang, J.and Zhao. Design of reliable control systems possessing actuator redundancies. *Journal of Guidance, Control, and Dynamics*, 23(4), 2000.

[17] T. Johansen and T. Fossen. Control allocation - a survey. *Automatica*, pages 1087–1103, 2013.

[18] C. Miller. Nonlinear dynamic inversion baseline control law: Architecture and performance predictions, 2011.

[19] M. Oppenheimer. Control allocation for over-actuated systems. In *2006 14th Mediterranean Conference on Control and Automation*. IEEE, 2006.

[20] J.A.M. Petersen and M. Bodson. Constrained quadratic programming techniques for control allocation. *IEEE Transactions on Control Systems Technology*, 14(1):91–98, 2006.

[21] F. Prochazka, H. Eduardo, and S. Klein. Integrated fault-tolerant control of an over-actuated aircraft using optimal control allocation and robust sliding mode observers. In *2018 2nd IEEE Conference on Control Technology and Applications*. IEEE, forthcoming.

[22] T. Ritz. Development of a model for the flight control of a hybrid unmanned aerial vehicle. unpublished thesis, 2018.

[23] H. H. Rosenbrock and A. G. J. MacFarlane. State-space and multivariable theory. *IEEE Transactions on Systems, Man, and Cybernetics*, 1972.

[24] SESAR. European drones outlook study. Report, 2016.

[25] B. Stevens, F. Lewis, and E. Johnson. *Aircraft control and simulation: Dynamics, controls design, and autonomous systems*. Third edition edition, 2016.

[26] E. van Oort. *Adaptive backstepping control and safety analysis for modern fighter aircraft*. PhD thesis, [S.l.], 2011.

[27] Y. Zhang and J. Jiang. Bibliographical review on reconfigurable fault-tolerant control systems. *Annual Reviews in Control*, 32(2):229–252, 2008.

[28] Y. Zhang, V. Suresh, B. Jiang, and D. Theilliol. Reconfigurable control allocation against aircraft control effector failures. In *2007 IEEE International Conference on Control Applications*, pages 1197–1202. IEEE, 2007.